Principles and promise of Fabry–Perot resonators at terahertz frequencies

R. Braakman[1,a] and G. A. Blake[2,b]
[1]*Division of Chemistry and Chemical Engineering, California Institute of Technology, 1200 E. California Blvd., Pasadena, California 91125, USA*
[2]*Division of Geological and Planetary Sciences, California Institute of Technology, 1200 E. California Blvd., Pasadena, California 91125, USA*

(Received 8 October 2010; accepted 31 January 2011; published online 17 March 2011)

Fabry–Perot resonators have tremendous potential to enhance the sensitivity of spectroscopic systems at terahertz (THz) frequencies. Increasing sensitivity will be of benefit in compensating for the relatively low power of current high resolution continuous wave THz radiation techniques, and to fully express the potential of THz spectroscopy as source power increases. Improved sensitivities, and thus scanning speeds, will allow detailed studies of the complex vibration-rotation-tunneling dynamics that large molecules show at THz wavelengths, and will be especially important in studying more elusive, transient species such as those present in planetary atmospheres and the interstellar medium. Coupling radiation into the cavity presents unique challenges at THz frequencies, however, meaning that the cavity configurations common in neighboring frequency domains cannot simply be translated. Instead, novel constructions are needed. Here we present a resonator design in which wire-grid polarizers serve as the input and output coupling mirrors. Using this configuration, Q-factors of a few times 10^5 are achieved near 0.3 THz. To aid future investigations, the parameter space that limits the quality of the cavity is explored and paths to improved performance highlighted. Lastly, the performance of polarizer cavity-based Fourier transform (FT) THz spectrometers is discussed, in particular those design optimizations that should allow for the construction of THz instrumentation that rivals and eventually surpasses the sensitivities achieved with modern FT-microwave cavity spectrometers. © *2011 American Institute of Physics*. [doi:10.1063/1.3560771]

I. INTRODUCTION

Spectroscopy at terahertz (THz) frequencies, also known as submillimeter-wave or far-infrared spectroscopy (and broadly defined as covering the 0.1–10 THz span), has been rapidly expanding over the last two decades and has applications in a great variety of fields, from remote sensing in astronomical and atmospheric settings, to the biological and medical sciences, to homeland security.[1–3] Time-domain techniques in particular have seen great advances in the sensitivity and spectral coverage that can be achieved in recent years,[3] but these techniques are limited in their achievable spectral resolution. In THz time domain spectroscopy (TDS), for example, a broadband THz field is generated by the illumination of photoconducting devices or suitable nonlinear optical materials (or more recently by the creation of laser-induced plasmas) with ultrashort femtosecond (fs) near-infrared laser pulses.[3] The THz electric field is then recorded in the time-domain using small portions of the same fs pulses, typically with beam splitters and an optical delay line; and the achievable spectral resolution is limited either by the length of the delay line or, ultimately, by the repetition rate of the laser—usually on the order $\gtrsim$80 MHz.

The most commonly used methods for generating high resolution continuous wave (CW) THz radiation in spectroscopic laboratories or astronomical observatories operate either by up-conversion through harmonic multiplication of microwave radiation, or down-conversion through difference frequency mixing of two narrow-band IR lasers on a photomixing chip. Both of these methods, however, are currently limited to power levels on the order $\lesssim$10 μW or (typically much) less at higher THz frequencies,[4–6] necessitating highly sensitive detectors and other techniques to improve the overall system sensitivity.

These limitations are especially central to the study of chemical species relevant to interstellar or atmospheric settings, where THz spectroscopy is expected to greatly advance our understanding in coming years. Conditions in the interstellar medium, for example, allow for the existence and survival of species that can be difficult to create in the gas phase on Earth; for example, transient species such as complex ions or radicals,[7,8] or molecules that are difficult to volatilize such as large organic acids. Various laser or high temperature induced reactions/vaporization techniques combined with supersonic molecular beam expansions that decrease the reaction or interaction opportunities do, in some cases, allow such difficult targets to be studied.[9,10] However, due to the low abundances of the species under investigation using such techniques, all methods to increase sensitivity should be explored.

Fabry–Perot cavity resonators provide an attractive method to increase the sensitivity of a spectroscopic system, as they allow a major increase in the path length and thus the fraction of light a medium can absorb. Increasing the path length of the light also increases the residence time of the photons in the cavity, and accurate measurement of

[a]Author to whom correspondence should be addressed. Current address: Santa Fe Institute, 1399 Hyde Park Road, Santa Fe, NM 87501, USA. Electronic mail: rogier@santafe.edu.
[b]Electronic mail: gab@gps.caltech.edu.

variations in this time forms the basis for cavity ringdown spectroscopy, which achieves great sensitivities and is widely applied at visible and infrared wavelengths.[11] At the (much) longer wavelengths of the MW and THz domains, however, the design of high reflectivity, low-loss mirrors with easy input/output coupling presents a more significant challenge.

A second route to increasing sensitivities that has seen widespread use, and for which cavities are also a central feature, is through the recording of the free induction decay (FID) of a rotational or low-energy torsional transition as a time-domain signal using heterodyne detection (with a Fourier transform serving to produce the frequency domain spectrum). Supersonic-jet expansions dramatically increase the effectiveness of this method at MW frequencies. The collision-free expansion suppresses long range interactions and dephasing of the coherent radiation field, which in turn allows easier recording of the lengthy FID, creating narrower and more intense lines, and the simultaneous cooling of the sample drives the population into the lowest states, which increases the fraction of the sample that can be excited. Cavities provide an ideal setting for supersonic-expansions as they can be designed to match the geometry of the beam while maintaining an open nature than can be easily (vacuum) pumped to allow high repetition rates. This technique allows remarkable sensitivities and serves at the basis of "Balle–Flygare" or Fourier transform microwave (FT-MW) systems that are widely used around the globe.[12–14]

In this paper, we explore the use of resonant Fabry–Perot cavities at millimeter and THz frequencies. Compared to the IR, cavity design at THz frequencies suffers from similar challenges as it does in the microwave domain, and thus the ultimate goal of this work is to build toward a THz analog (i.e., FT-THz) of the FT-MW systems that commonly operate at 1–40 GHz. In achieving a high sensitivity FT-THz system, the cavity is of central importance as, in addition to the principles outlined above, its nature and quality will impact various aspects of the system, including path length, detector requirements (sensitivity, bandwidth), source power levels, etc. As will be discussed in more detail in the next section, however, THz frequencies provides unique challenges in the use of resonant cavities as not only common IR input/output coupling schemes but also those used at MW frequencies translate poorly to this domain. For example, hole output coupling scales poorly with frequency,[15] and dielectric diplexer-mirror cavities have good performance but can be complex to align and tune for frequency agile experiments.[16,17]

Here, the use of wire grid polarizers as input and output coupling mirrors is investigated. Due to the nature of the optics being used and the low powers that are available at THz frequencies, accurate consideration of the Gaussian nature of the radiation beam and the coupling of the beam(s) to the various spectrometer optics is important. After discussing how these aspects constrain the design of our instrument, we consider the fundamental limitations for THz cavities, and compare these theoretical results to experimental data of the proposed setups. Finally, we discuss how the performance of these cavities may be optimized and how, when combined with pulsed radiation sources and molecular beam expansions, they should allow for FT-THz systems that can compete favorably with FT-MW systems.

II. CAVITY DESIGN

In this section we describe how the Gaussian nature of the beam and the use of wire-grid polarizers as input/output coupling mirrors affects cavity design.

A. Gaussian beams

In the limit where the wavelength is negligible relative to the size of the optical elements, geometrical optics design approaches work well. Where the wavelength is comparable to the size of the optics, however, diffraction effect dominate the performance of an optical system. The intermediate domain, where the size of the optics is large—but not infinite—compared to the wavelength, the power distribution in the beam needs to be considered carefully. In THz spectroscopy, with wavelengths of ~0.1–1 mm, this last aspect is critical, especially in a cavity resonator where small losses at the tails of the power distribution can add up over many roundtrips. The power density distribution across the width of the beam has a Gaussian profile and is given by[18]

$$P(r) = P(0)e^{-2(r/\omega)^2}, \tag{1}$$

where r is the distance from the propagation axis and ω (the "beam radius") is the distance from the propagation axis to that point where the electric field has fallen off to $1/e$ of its value on-axis. Early in the study of the mode structure of resonators, it was shown that confocal spherical systems (where $L=2F$, L being the length of the cavity and F the focal length of the mirror) are far superior compared to plane mirror systems in terms of diffraction (or spill-over) losses.[19] In confocal cavities, Gaussian beams have the property that the power distribution widens from the midposition of the cavity toward the spherical reflectors, where the curved equiphase wave front matches the metallic surface, and the radius and radius of curvature of the beam are described by[18]

$$\omega = \omega_0\left[1+\left(\frac{\lambda z}{\pi\omega_0^2}\right)^2\right]^{0.5}, \tag{2}$$

$$R = z+\frac{1}{z}\left(\frac{\pi\omega_0^2}{\lambda}\right)^2, \tag{3}$$

where z is distance from the confocal center along the (symmetry) axis of propagation, ω_0 is the minimal beam radius (=beam waist) that occurs at $z=0$, and λ is the wavelength of the radiation. Confocal cavities have several nice design properties. As we know from standard optics the radius of curvature of a spherical mirror equals twice the focal length (or, $R=2F$), and the focal length of the mirror is thus the fundamental determinant of the Gaussian mode structure of the cavity through the simple relationships[18]

$$\omega_0 = \left(\frac{\lambda F}{\pi}\right)^{0.5}, \tag{4}$$

$$\omega_m = \sqrt{2}\omega_0, \tag{5}$$

where ω_m is the beam radius at the mirror. Relationship (5) follows from the fact that at the mirror $z = F$. Knowing the beam diameters from the focal length of the mirror, it is thus easy to design optical systems with diameters sufficiently large to ensure the diffraction loss is indeed negligible compared to other losses in the system. Generally, optics with a diameter more than 4 times the beam waist, $D_{opt} = 2r_{opt} > 4\omega$ are sufficient to make diffraction loss negligible.

Operating in this domain allows for two basic designs: a confocal cavity consisting of two spherical mirrors spaced at a distance equal to the sum of their focal lengths, and a semiconfocal cavity consisting of a spherical mirror and a planar mirror spaced at a distance equal to the focal length of the spherical mirror. The former configuration is the most common arrangement in both MW (Ref. 13) and IR (Ref. 11) cavity spectrometers. For the design presented here, however, flat wire-grid polarizers are used as the input/output coupling mirrors, and this naturally leads to an exploration of semiconfocal THz cavities.

B. Cavity configuration

Fabry–Perot resonant cavities are commonly used in spectroscopic setups over a wide range of frequencies. The two most closely related frequency domains that we will consider here for suggestions on how to extend cavity-enhanced techniques into the THz range are the neighboring MW and IR regions. At infrared wavelengths, input/output coupling mirrors generally consist of dielectric stacks that are composed of multiple thin layers of films with different refractive indices. Such dielectric mirrors function on the principle of optical interference, with the thickness and refractive index of the different layers chosen such that the reflected light from different layers constructively interfere, which allows the construction of mirrors with very high reflectivity and exceptionally low loss per pass, while still transmitting a small fraction of radiation. Due to the much longer wavelengths, this is technologically difficult to achieve at THz frequencies, and no such dielectrics currently exist that function at room temperature and wavelengths beyond 30–40 μm. Metallic mirrors, with only a small conductance loss in the surface, provide a material that is, in principle, capable of achieving the high reflectivity required for the type of experiments discussed here. However, metallic mirrors do not transmit radiation, thus requiring another method of coupling the radiation into the cavity. At microwave frequencies, this problem is surmounted by coupling the radiation into the cavity using either a coaxially fed antenna mounted inside the mirror(s),[13] or a waveguide butted against an iris in one of the mirrors.[12] Due to the long wavelengths of MW radiation, it is not difficult to minimize the impact of these cavity 'imperfections', but because THz wavelengths are two orders of magnitude smaller, it is difficult to employ these coupling methods without severely negatively impacting the quality factor of the cavity.

These factors suggest an exploration of THz cavities that use wire-grid polarizers as input/output coupling mirrors. Any electric field component parallel to a metal wire will cause electrons to flow along the wire, turning it into a reflective/diffractive element. A wire-grid polarizer consists of an array of such conducting metal wires, with both the spacing between the wires g and the diameter of the wires d significantly less than half the wavelength: $g << \lambda/2$, $d < g$. Under these conditions, the reactive shunt impedance of the grid is significantly less than the characteristic impedance of free space, resulting in almost complete reflection of the incident electric field component parallel to the grid.[18] A small amount of radiation does leak through the grid, however, providing exactly the characteristics that are needed for coupling radiation in to and out of a standing-wave cavity. The use of a wire-grid does affect the configuration of the cavity, however, as it provides a flat surface rather than the spherical mirrors used in traditional confocal cavities.

A basic semiconfocal cavity is the first configuration considered, and is outlined in Fig. 1. It consists of a wire-grid polarizer opposite a spherical metallic mirror, where the polarizer acts as both the input and output coupling mirror. A 50:50 beam splitter outside the cavity serves to redirect the output beam toward the detector. The two passes across the beam splitter are costly, however, as 75% of the power is lost even before considering any cavity losses. As shall be demonstrated in the experimental results section, the fact that the input/output beams travel the same path has additional, more significant downsides, and we therefore considered an alternate configuration that separates the input and output beams altogether.

The cavity seen in Fig. 2 is a variation on the basic semiconfocal cavity. Now the beam couples in to and out of the cavity through separate wire-grid polarizers, which is achieved by rotating the input and output "arms" of the cavity apart by using an off-axis parabolic mirror rather than a spherical mirror. This configuration circumvents the need for a beam splitter, maintaining a higher fraction of the source power and generally simplifying the cavity output spectrum as is shown below. Though the cavity is confocal in nature and has the associated advantages in terms of diffraction losses, it is important that the two book-ended flat mirrors are perpendicular to the symmetry-axis of propagation (and

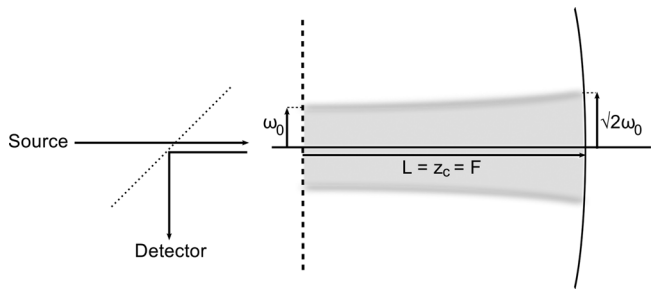

FIG. 1. A THz cavity consisting of a basic semiconfocal Fabry–Perot resonator. The cavity consists of a wire-grid polarizer that acts as both the input and output coupling mirror, and a spherical mirror used to refocus the beam and minimize diffraction loss. In gray is the resonantly enhanced THz beam, with the confocal length of the beam equal to the focal length of the cavity and the beam waist indicated by ω_0. The metal wires of the grid and the E-field of the beam are aligned parallel to each other, creating maximally reflecting conditions. A 50:50 beam splitter is employed to redirect the output-coupling beam to the detector.

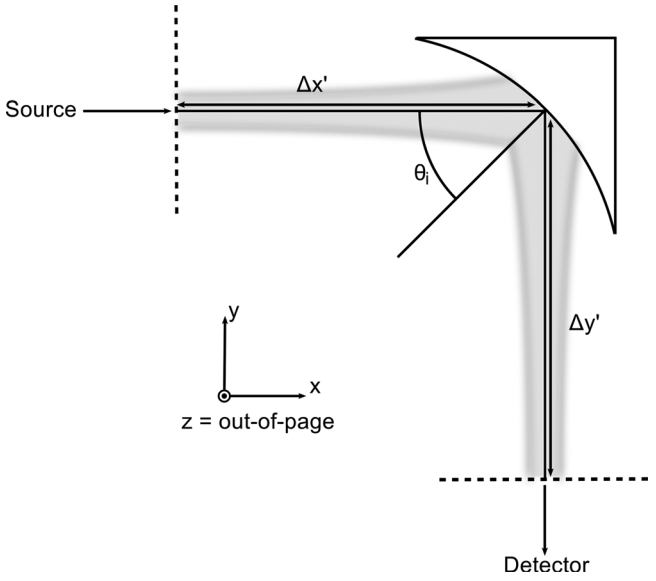

FIG. 2. A THz cavity consisting of an "off-axis semiconfocal" Fabry–Perot resonator. This cavity is, in principle, the same as that shown in Fig. 1, with the significant difference that the output beam is directed away from the input beam by an off-axis parabolic mirror. A curved off-axis mirror refocuses the beam and minimizes diffraction losses compared to a parallel plate resonator. Two separate wire-grid polarizers, each positioned at the focal length of the mirror ($\Delta x' = \Delta y' = F$, maintaining confocal conditions) are now used to couple the beam in to and out of the cavity, which circumvents the need for a beam splitter. In the view shown, both the E-field of the beam and the wires of the polarizers are aligned along the z-axis, perpendicular to the plane in which the arms are rotated. The angle of incidence of the beam on the surface of the parabolic mirror is indicated by θ_i.

effectively parallel to each other) to prevent "walk-off" losses. A parabolic mirror of any angle can be used in this arrangement, but because of their ready availability and easy alignment we tested the principles of "off-axis semiconfocal" cavities using a 90° parabolic mirror.

Before comparing the THz properties the two cavities discussed above, it is first useful to consider how the quality of the cavity depends on the nature of the optics used. The quality (Q) factor of a cavity, which describes the ratio of power stored in the cavity to the rate of power dissipation, is useful for this purpose. The "loaded Q" (including coupling losses) can be measured from the spectrum through[19]

$$Q_L = \frac{\nu}{\Delta\nu}, \tag{6}$$

where ν and $\Delta\nu$ are the frequency and width of the cavity mode, respectively. The Q factor is further related to the path length and the ringdown time τ of the cavity by

$$L_{\text{eff}} = \tau c = \frac{Q\lambda}{2\pi}. \tag{7}$$

Equation (7) shows clearly how the sensitivity depends directly on the Q factor.

III. CAVITY LOSSES AND THEORETICAL *Q* FACTOR

The standard equation for the Q factor of a cavity where the losses are very small is[19]

$$Q = \frac{2\pi L}{\lambda\alpha_m}, \tag{8}$$

where L is length of the cavity, λ is the wavelength of the photons, and α_m is the sum of the losses at the mirror (with negligible diffraction loss this is the sum of reflection and absorption losses). Equation (8) assumes that the system consists of two equivalent mirrors and cavity quality is thus a reflection of the amount of power lost as the photons travel down one *length* of the cavity. Since this condition holds for most cavities used in ring-down instruments this equation correctly calculates the theoretical Q factor. However, as the THz cavities under consideration consist of more than two mirrors that are also nonequivalent, a more general form is

$$Q = \frac{4\pi L}{\lambda\alpha_{\text{RT}}}, \tag{9}$$

where Q is now proportional to the ratio of the round trip length ($2L$) of the cavity to the total loss per round trip α_{RT}. For a round trip in a cavity with two equivalent mirrors, the round trip loss is simply $\alpha_{\text{RT}} = 2\alpha_m$, which returns Eq. (8), as expected. The theoretical Q factor for the polarizer-mirror cavities under consideration can now be calculated by tabulating the loss terms at each element in the cavity.

A. Cavity losses

In both of the cavities tested here the radiation passes across wire-grid polarizers and spherical or parabolic mirrors. The theoretical loss at each reflective element must therefore be calculated and summed appropriately to determine the total loss and theoretical Q factor. The goal here is to formulate all losses in terms of the fundamental physical properties of the cavity elements, that is the resistivity (or conductivity) of the metals, the diameter and spacing of the wires in the polarizers, the wavelength of the radiation and the angles of incidence at the mirrors.

1. Wire-grid polarizers

We begin by considering the loss at the wire grid polarizers, each of which consists of a fine array of metal wires. When reflecting off a polarizer of this nature, the radiation beam can lose power through imperfect reflection or through resistive absorption by the metal. The absorption (or conductance) loss for a closely spaced grid of metal wires at normal incidence can be calculated using[18]

$$\alpha_{c,\text{wg}} = \mathbf{R}\left(\frac{4R_l}{Z_0}\right) \tag{10}$$

where $\mathbf{R}$ is the reflectivity of the grid, R_l is its effective loss resistance and Z_0 is the impedance of free space ($Z_0 = \mu_0 c \sim 376.73\ \Omega$). The surface resistance of a metal is given by $R_s = \sqrt{\pi\nu\mu_0\rho}$, where μ_0 is the permeability of free space and ρ the resistivity of the metal. The gridlike nature of the metal is then taken into account by multiplying with the factor $2g/u$,[18] where where g and u are the spacing and circumference of the wires, respectively. Together, this gives the loss resistance of the grid:

$$R_l = R_s \frac{2g}{u} = \sqrt{\frac{2g\rho Z_0}{\pi d\lambda}}. \tag{11}$$

In the limit where the reflectivity **R** approaches unity (a requirement for a high quality cavity), the absorption loss is thus given by

$$\alpha_{c,wg} = 4\sqrt{\frac{2g\rho}{\pi d Z_0 \lambda}}. \tag{12}$$

Next, the reflectivity of the grid is given by[18,20]

$$\mathbf{R} = \frac{1}{|1 + 2Z_g/Z_0|^2} = \frac{1}{(1 + 2R_l/Z_0)^2 + (2X_g/Z_0)^2}, \tag{13}$$

where Z_g and X_g are the impedance and reactance of the grid, respectively. The grid reactance is related to the grid capacitance through $X_g = -1/(2\pi\nu C_g)$. The grid capacitance can be determined from the capacitance of the two central parallel wires in the grid, which is given by[21]

$$C_g = \frac{2\pi\varepsilon l}{\cosh^{-1}\left(\frac{g^2 - 2a^2}{2a^2}\right)}, \tag{14}$$

where ε is the permittivity of the metal, l is the length of the wire, and $a = d/2$ is the radius of the wire. Inserting various terms, Eq. (13) can then be rewritten to

$$\mathbf{R} = \frac{1}{\left(1 + \sqrt{8g\rho/\pi d Z_0 \lambda}\right)^2 + \left(\lambda \ln\left[2g^2/d^2 - 1 + (2g/d)\sqrt{g^2/d^2 - 1}\right]/2\pi^2 l\right)^2}. \tag{15}$$

In practical terms, however, Eqs. (13) and (15) can be significantly simplified. When the basic requirements of high reflectivity for a grid ($g << \lambda/2$, $d < g$) are met, and a grid diameter sufficient to eliminate diffraction loss is chosen, it turns out that at THz frequencies we are in the limit where both R_l, $X_g << Z_0$. As a result, the second term in Eq. (13) becomes negligible, and we can simplify Eq. (13) to

$$\mathbf{R} = 1 - \left(\frac{4R_l}{Z_0}\right). \tag{16}$$

Without choosing the parameters g, d, and l in a way that completely disrupts the functioning of the cavity, the reactance will always be very small, $X_g \ll Z_0$. As such the only way to move out of the limit above is to decrease the loss resistance to the point where $R_l \ll X_g \ll Z_0$, and as $d/g > 1$ must hold, the only way to achieve this is by significantly decreasing the resistivity ρ. To indicate how well this limit holds for THz cavities, we examined the wire-grids tested in this work. We tested two different tungsten wire-grids near 0.3 THz (see next section) and for those grids the true value for the total loss (absorption + reflection) deviates from the limit above by a factor on the order of 10^{-5}. Even for a resistivity 3 orders of magnitude lower than its actual room temperature value the deviations would only be on the order of 5%. Such resistivities could be achievable by cooling aluminum to temperatures $T < 30$ K, and for tungsten and gold cannot be reached. Furthermore, as X_g decreases linearly with frequency while R_l rises with the square root of the frequency, we are increasingly in this limit at higher THz frequencies. In other words, without resorting to superconducting wire-grids, the reflection loss of any practical wire-grid based THz cavity equals its absorption loss, and the total loss of the grid is given by

$$\alpha_{\mathrm{wg}} = \alpha_{c,\mathrm{wg}} + \alpha_r = \frac{8R_l}{Z_0} = 8\sqrt{\frac{2g\rho}{\pi d Z_0 \lambda}}. \tag{17}$$

2. Parabolic metal mirrors

For a parabolic metal mirror the reflecting beam can lose power through resistive absorption by the metal, and because off-axis reflection alters both the shape and polarization content of the beam. Taking into account off-axis reflection and using the surface resistance as above, the resistive absorption in the $E_{||}$ component of the beam is[18]

$$\alpha_c = \frac{4}{\cos\theta_i}\left(\frac{R_s}{Z_0}\right) = \frac{4}{\cos\theta_i}\sqrt{\frac{\pi\rho}{Z_0\lambda}}, \tag{18}$$

where θ_i is the angle of incidence as shown in Fig. 2. For the cavities tested here, the prefactor $(1/\cos\theta_i)$ equals 1 for the basic semiconfocal cavity ($\theta_i = 0$) and $\sqrt{2}$ for the off-axis cavity ($\theta_i = 45°$). The losses due to beam distortion and cross-polarization of the beam are due to the Gaussian nature of the beam reflecting off a curved surface, and are given by[18]

$$\alpha_{\mathrm{bd}} = \frac{\omega_m^2 \tan\theta_i}{8F^2}, \tag{19}$$

$$\alpha_{\mathrm{cp}} = \frac{\omega_m^2 \tan^2\theta_i}{4F^2}, \tag{20}$$

where ω_m is the beam waist at the mirror, θ_i is the angle of incidence of the beam, and F is the focal length of the mirror. Since $\omega_m^2 = 2\omega_0^2 = 2\lambda F/\pi$ [see Eqs. (4), (5)], the two equations above can be combined and simplified to give the "beam-alteration" loss

$$\alpha_{\mathrm{ba}} = \frac{\lambda}{2\pi F}\left(\frac{\tan\,\theta_i}{2} + \tan^2\,\theta_i\right). \tag{21}$$

For both of the cavities here, this equation simplifies further. For the classic semiconfocal cavity $\theta_i = 0$, which reduces the beam alteration loss to zero. For the straight angle off-axis semiconfocal cavity, the incidence angle of $\theta_i = 45°$ gives $\tan\theta_i = \tan^2\theta_i = 1$, which simplifies the beam alteration loss to

$$\alpha_{\mathrm{ba}} = \frac{3\lambda}{4\pi F}. \tag{22}$$

The total loss after reflection off a metal off-axis parabolic mirror is again simply the sum of the conduction and beam alteration losses or $\alpha_{\mathrm{oam}} = \alpha_c + \alpha_{\mathrm{ba}}$.

B. Theoretical summary

Several features are immediately obvious when looking at the loss terms of the various optics. Universal to all optics considered here is the effect of the resistivity of the metal, with better conductors (lower resistivity) leading to higher reflectivity for wire-grids and lower absorption losses in both wire-grids and parabolic mirrors. For wire-grid polarizers it is further seen that both absorption and reflection losses are dependent on the ratio of the spacing to the diameter of the wires. As long as the requirements for high reflectivity of the grid are met ($g << \lambda/2$, $d < g$), it thus pays to go with the widest diameter wires possible.

For parabolic mirrors we find that both the angle of incidence and the focal length are important factors in the magnitude of the losses. Increasing the angle of incidence increases both the conductance and beam alteration losses. These losses can partly be compensated for by using a mirror with a longer focal length. In doing so, it is important to use optics of sufficient diameter so that the relative diffraction losses in the system remain ~ 0, as we know from Eqs. (4) and (5) that the diameter of the THz beam increases with the square root of the focal length. With this caveat, increasing the focal length has a second advantage, as we saw in Eq. (9) that the Q factor is directly proportional to the length of the cavity; increasing this length thus compensates for *all* cavity losses.

The effect of the wavelength on losses is less straightforward. The total loss for wire-grids and the conductance loss for parabolic mirrors both decrease with the square root of the wavelength, while the beam alteration loss for parabolic mirrors increases linearly with the wavelength. On the other hand, the Q factor is inversely proportional to the wavelength, and thus, as with increasing the size of the cavity, going to higher THz frequencies compensates for *all* cavity losses. Another way to understand this is from Eq. (6) in which we see that for a constant *absolute* mode width, its *relative* width decreases as the frequency increases.

Using the equations above it is possible to model in detail the dependence of the Q factor on the properties of the cavity optics and radiation beam and optimize the design for a specific purpose. A full exploration and optimization of many cavity designs is beyond the scope of the current work, the goal here is to simply to test the principles of semiconfocal Fabry–Perot THz resonators of either on-axis or off-axis design, and to evaluate the experimental results in terms of the theoretical framework outlined above.

IV. EXPERIMENTAL RESULTS

Both semiconfocal cavities were studied using a swept frequency source at a wavelength of 1 mm (= 300 GHz or 0.3 THz). The radiation was generated using a 12.5–20 GHz Wiltron microwave source followed by a room-temperature solid state multiplier chain ($\times$ 2$\times$ 3 $\times$ 3) that generates radiation in the 225–360 GHz range. Simple lenses were used to refocus the radiation and position the beam waist at the input mirror, where it couples into the Gaussian modes of the cavity. The radiation exiting the cavity was again refocused using simple lenses and sent to the detector, which consisted of a combination of a Virginia Diodes Shottky diode detector and Stanford lock-in amplifier. The experiment was run in AM mode to record the signal as absolute power versus frequency.

First the basic semiconfocal cavity as outlined above in Fig. 1 was tested by sweeping the source near a frequency of 300 GHz. The optics consisted of a tungsten [$\rho = 5.28 \times 10^{-8}$ Ωm at 20 °C (Ref. 22)] wire-grid polarizer (model G45 $\times$ 10 purchased from Microtech Instruments), with a diameter of 10 cm and made of wires that are 10 μm wide and spaced by 45 μm, and a spherical gold [$\rho = 2.21 \times 10^{-8}$ Ωm at 20 °C (Ref. 22)] mirror with an effective focal length of 30 cm and a diameter of 15 cm. At 300 GHz (= 1 mm) these numbers give losses of $\alpha_{\mathrm{wg}} = 5.1 \times 10^{-3}$ at the wire-grid, and $\alpha_{\mathrm{oam}} = \alpha_c + \alpha_{\mathrm{ba}} = 1.7 \times 10^{-3} + 0 = 1.7 \times 10^{-3}$ at the spherical mirror. The beam radius is 9.7 mm at the wire-grid and 1.4 cm at the spherical mirror making diffraction losses negligible. In total we have a round trip loss of $\alpha_{\mathrm{rt}} = 6.8 \times 10^{-3}$, and a theoretical Q factor of $Q = 5.6\times 10^5$.

The measured spectrum can be seen in Fig. 3. The fundamental TEM_{00} modes (labeled M) completely extinguish the signal at the detector, as expected for a critically coupled reflection cavity.[12] The width of these modes is 2.2 MHz, which corresponds to a measured $Q_L = 1.4 \times 10^5$ and is approximately one quarter of the theoretical maximum. However, as can be seen the spectrum is complicated by the additional presence of several higher order (TEM_{mn}) modes. The different modes are impacted to varying degrees by phase shifts and other imperfections of the cavity, which can lead to confusion during alignment and optimization. In addition, the spectrum is also marred by a prominent sinusoidal baseline variation, which is the result of etalons between the various optical elements in the system.

The easiest solution to address these issues is to separate the input and output beams of the cavity, as is in the arrangement shown in Fig. 2. The optics used consisted of a tungsten wire-grid polarizer (model G50 $\times$ 20) with dimensions $g = 50$ μm and $d = 20$ μm as input mirror, a second tungsten wire-grid polarizer (model G45 $\times$ 10) with dimensions $g = 45$ μm and $d = 10$ μm as output mirror, and a 90° off-axis parabolic mirror made of aluminum [$\rho = 2.65 \times 10^{-8}$ Ωm at 20 °C (Ref. 22)] with an effective focal length of 15 cm. At 300 GHz these numbers give losses of α_{wg}

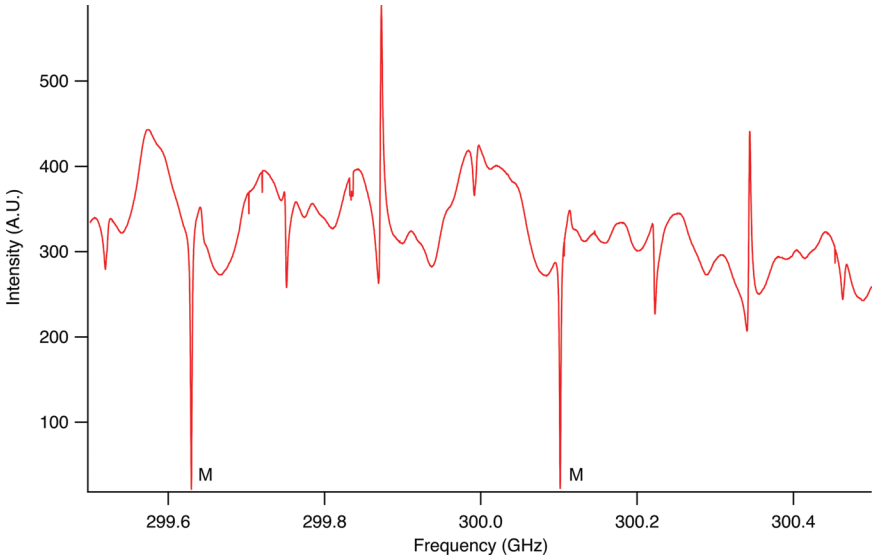

FIG. 3. (Color online) Frequency spectrum for a semiconfocal cavity arrangement such as seen in Fig. 1, recorded in AM mode. The critically coupled fundamental TEM_{00} modes are labeled M, and several higher order TEM_{mn} can also be seen. The width of the TEM_{00} modes is 2.2 MHz, which corresponds to a measured $Q_L = 1.4 \times 10^5$, approximately one quarter of the theoretical limit of $Q = 5.6 \times 10^5$. Standing waves between the various optics (etalons) are also prominent in the spectrum.

$= 5.1 \times 10^{-3}$ (G45 × 10) and $\alpha_{wg} = 3.8 \times 10^{-3}$ (G50 × 20) at the wire-grids, and a loss of $\alpha_{oam} = \alpha_c + \alpha_{ba} = 2.7 \times 10^{-3} + 1.6 \times 10^{-3} = 4.2 \times 10^{-3}$ at the parabolic mirror. The total round trip loss is $\alpha_{rt} = 5.1 \times 10^{-3} + 3.8 \times 10^{-3} + (2 \times 4.2 \times 10^{-3}) = 1.7 \times 10^{-2}$, and the theoretical Q factor is $Q = 2.2 \times 10^5$.

The spectrum resulting from scanning across this cavity can be seen in Fig. 4, and it immediately shows the advantages of operating in this configuration. Separating the input and output beams selectively filters out both the higher order TEM_{mn} modes and etalons, leaving only the TEM_{00} modes and a flat baseline, which eases alignment and optimization. Comparing to the theoretical capabilities of this cavity, the width of the modes in Fig. 4 is $\Delta\nu = 2.0$ MHz, which gives a Q factor of $Q_L = 1.5 \times 10^5$, an effective path length of $L_{eff} = 24$ m and a ringdown time of $\tau = 0.8$ μs. We see that the measured Q factor is very close to the theoretical limit and is significantly limited by the off-axis parabolic mirror (nearly half the losses arising there).

V. DISCUSSION

In the present work a simple, highly frequency agile method for constructing Fabry–Perot resonators at THz frequencies is demonstrated. The basic design employs wire-grid polarizers as the input/output coupling mirrors, with an off-axis parabolic mirror serving to separate and refocus the input and output beams.

A. Cavity performance

Separating input and output beams allows the selective transmission of the fundamental cavity modes similar to what is achieved with perpendicular pairs of L-shaped $\lambda/4$ antennas in modern FT-MW machines.[13] A significant advantage of the configuration presented here is that an even broader coverage than the already impressive range of FT-MW machines (more than 3 octaves using perpendicular antenna pairs[13]) should be possible without hardware changes. The effectiveness of antenna coupling is ultimately

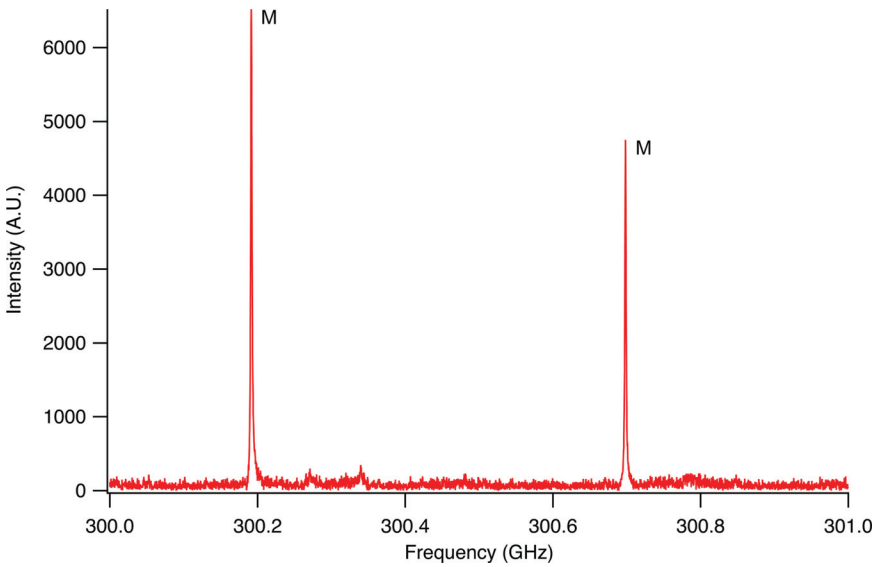

FIG. 4. (Color online) Frequency spectrum for an off-axis cavity arrangement such as that seen in Fig. 2, recorded in AM mode. Separation of the input and output beams significantly simplifies the spectrum, with both the higher order TEM_{mn} modes and etalon effects filtered out of the spectrum, leaving only the fundamental TEM_{00} modes (labeled M) on an otherwise flat baseline. The width of the modes is 2.0 MHz, corresponding to $Q_L = 1.5 \times 10^5$. This is close to the theoretical limit of $Q = 2.2 \times 10^5$.

limited by the size of the antenna relative to the wavelength of the radiation, and eventually falls off when the system is tuned far from its optimal frequency. This is not the case for wire-grid based cavities where the coupling elements simultaneously serve as the mirrors of the system. Thus, for a given wire-grid it should, in principle, be possible to efficiently generate high electric-field conditions over the entire range in which the quality factor remains high. For the off-axis cavity tested here, this implies a very wide range indeed. Increasing the frequency tenfold, from 0.3 to 3.0 THz, and keeping all other parameters fixed, decreases the theoretical maximum for the Q factor decreases only threefold. Even at 10 THz the Q factor is still one-fifth of the value at 0.3 THz. Thus, if appropriate Gaussian telescopes are used to fix the distances from the emitter/detector to the cavity, fixing the position of the beam waists at the input/output coupling mirrors, a cavity thus constructed should be able to maintain a high quality, and operate, over many THz of frequency space without any modifications.

Further, the size of all loss terms for the optics used in the cavity have been derived, which allows a determination of the theoretical Q factor in terms of the fundamental physical properties of the cavity elements. Such calculations also give direct insights into the limiting factors for the cavity quality for given conditions and suggest paths by which the performance may be improved. For the cavities we tested in this work, we find very similar Q factors, with $Q_L = 1.4 \times 10^5$ for the basic semiconfocal cavity and $Q_L = 1.5 \times 10^5$ for the off-axis semiconfocal cavity. The off-axis cavity is closer to its theoretical maximum than the basic version, but both operate at qualities very similar to the values of $Q_L \sim 1 - 2 \times 10^5$ at which modern FT-MW machines typically operate.[14] Both types of cavities can thus be used to enhance spectroscopic sensitivity, although, as shown in Figs. 3 and 4, the off-axis cavity has a much simpler spectrum which increases the ease of alignment, optimization and scanning.

Finally (and perhaps somewhat counter-intuitively), as was also shown in the experimental results section, nearly half of the losses in the off-axis configuration arise at the parabolic mirror, in which the angle of incidence and the focal length of the mirror loom large. As pointed about before, increasing the focal length also directly increases the Q factor. Indeed, simply decreasing the angle of incidence to a smaller 15° and switching to a gold parabolic mirror with a 30 cm focal length (equivalent to that used in the basic semiconfocal arrangement) gives an almost three times higher theoretical Q factor of 6.1×10^5 at 0.3 THz while maintaining a compact layout. This is nearly equivalent to that of the basic semiconfocal arrangement, but with the great advantages described above. Using wire-grids made of aluminum rather than tungsten and increasing the width relative to the spacing of the wires to $g/d = 2$ further increases the theoretical maximum to Q factor of 9.0×10^5. In conclusion, by pushing at the limits of off-axis semiconfocal cavities, path lengths of several hundred meters and ringdown times of several microseconds are within reach. As the ratio g/d must remain above 1, the largest future gains in the Q factor can be expected from lowering the resistivity of the metals used, and increasing the focal length of the parabolic mirror.

B. Sensitivity of pulsed FT systems at THz and MW frequencies

In addition to increasing the sensitivity of the spectroscopic system by increasing the path length and thus the lifetime of the photons in the experiment, further increases can be achieved by incorporating a high quality cavity in a pulsed Fourier transform (FT) system. At microwave frequencies, such FT-MW, or "Balle–Flygare", spectrometers are capable of very high sensitivities by combining high quality resonant cavities with pulsed radiation sources and molecular beams. In these systems, near $\pi/2$ microwave pulses are coupled into the cavity with a pulse length that is sufficiently short so that its Fourier components cover the frequency span of the cavity mode and with a temporal duration short compared to the rotational dephasing time of the coherent electric field in the cavity. Operating in this regime results in maximal polarization of the gas and allows the dephasing signal to be recorded in the time-domain via heterodyne detection, which allows significant increases in sensitivity beyond an increased path length. To evaluate the possible gain in sensitivity at THz frequencies by employing a THz analog of the Balle–Flygare system, we compare the theoretical sensitivity of an FT-THz system at the Q levels discussed above to the sensitivity of an FT-MW machine. Here, it is necessary to compare both the levels of the signal power coupling out of the cavity and the noise level of heterodyne detection at both frequencies.

Modern FT-MW machines rely on supersonic jet expansions to introduce sample into the system, but as we will compare different injection techniques below, we begin by examining how the system scales for a static gas cavity. The power of the molecular signal coupling out of a cavity completely filled with static gas is given by[23]

$$P_{\text{out}} = \frac{16}{9}\pi^2 Q_0 v_0 (|\langle a|\mu_z|b\rangle|\Delta N_0)^2 \pi \omega_0^2 L \times \left[\left(\frac{1}{\kappa E_0 \tau_p}\right)\int_0^{\kappa E_0 \tau_p} J_1(u)du\right]^2, \quad (23)$$

where v_0 is the frequency of the rotational transition, $\langle a|\mu_z|b\rangle$ is the electric transition dipole moment, ΔN_0 is the number density of emitters (that is the number of molecules per volume N/V multiplied by the fractional population difference between states n_0), ω_0 is the beam waist of the THz field in the cavity, L is the length of the cavity, $\kappa = (2/\hbar)\langle a|\mu_z|b\rangle$, $\mathbf{E}_0$ is half the maximum electric field amplitude in the cavity, τ_p is the microwave pulse length, and $\mathbf{J}_1(u)$ is the first order Bessel function. If we assume a transition with an equivalent dipole moment for both the THz and MW domains, and operate in the same optimal pulse regime (i.e., equal $\kappa E_0 \tau_p$ and at the maximum of the Bessel function), the *relative* output coupling power between domains for a cavity completely filled with static gas simplifies to

$$P_{\text{out}} \propto Q_0 v_0 \Delta N_0^2 \omega_0^2 L, \quad (24)$$

where the product $\omega_0^2 L$ describes the volume of the gas (of a given number density) that is emitting. Supersonic-jet injections generally do not completely fill the cavity, however,

and so we replace the product of the number density of emitters and volume $\Delta N_0^2 \omega_0^2 L$, with the total number of molecules N times the fractional population difference n_0. For the line of reasoning so far, and the simplification of Eq. (23), to be true, a certain minimum power level of THz radiation is needed and will be discussed below. The FT-MW power requirements are such that it is straightforward to achieve the necessary field strengths with commercial oscillators, and one of the long term principal challenges will be the continued development of higher power THz radiation sources. As the fraction of molecules that can be excited is dependent on the availability of photons, we should therefore insert a term p signifying the density of photons in the region where the radiation and molecular beams overlap. Additionally, for a given power level the number of photons scales linearly with inverse frequency, but we also see that total output coupled power scales linearly with frequency. Thus, for a similar pulse length, the product $v_0 p$ can be replaced by the amount of power coupling into the cavity P_{in}. Finally, then, we arrive at the relative output coupled power between THz and MW domains

$$P_{\text{out}} \propto Q_0 N \Delta n_0 P_{\text{in}}. \tag{25}$$

Thus, for a transitions with similar transition dipole moments and operating in the same experimental pulse regime, it is the Q factor, the total number of molecules in the beam N, the fractional population in the ground state n_0, and the power coupled into the cavity P_{in} that determines the relative output coupled power between the THz and MW frequency domains. As we saw above, the Q factors we achieve in this work are nearly equivalent to what is commonly achieved in FT-MW machines, and so the comparison ultimately comes down to a comparison of the last three terms in Eq. (25).

As mentioned, current MW systems have a significant advantage in available source power levels, and so, assuming similar coupling efficiencies, have a substantial advantage in terms of power coupled into the cavity P_{in}. On the other hand, the fractional population difference n_0 is a significant advantage at THz frequencies. Even at the low temperatures of supersonic jet expansions ($\sim 1-5$ K) the upper state of the low-energy rotational transitions at MW frequencies will have significant population, resulting in a small population difference. For mm-wave and THz transitions on the other, hand, most of the population will be in the ground state, resulting in a large population difference. As the cross-section of the radiation beam scales linearly with frequency, the total number of emitters N will be larger at MW frequencies, as the much wider beam will overlap with a larger fraction of the molecular beam. However, for a pinhole expansion the number density drops as $1/r^2$ (r is distance from nozzle), which means that the drop in molecules number can be compensated somewhat by placing the higher density regions of the expansion closer to the radiation beam and resulting in less than linear scaling with frequency. A further means to increase the number of molecules in FT-THz systems would be to move to slit jet expansions such as those employed in tunable far-infrared laser sideband studies of hydrogen bonded clusters.[24–26] In pulsed slit jet-expansions, the on-axis jet density drops as $1/r$, not $1/r^2$ as with pinhole expansions, but at the cost of much, much higher pumping speed requirements and significantly shorter Mach disk distances. Slit jets would fill only fill a small fraction of an FT-MW cavity, but due to the much narrower beams would be well matched to an FT-THz instrument and dramatically increase the total number of molecules in the radiation beam.

Slit jets have another advantage, which is that while pinhole jets expand in a three dimensional plume, slit jets essentially only expand in a two dimensional plane as the expansion along the slit is suppressed. This reduces the Doppler broadening if the slit is aligned with the propagation axis of the THz beam, and results in much narrower and more intense lines. Measurements of the lowest Σ bending state of the ArHCl cluster near 0.8 THz in a slit jet expansion, for example, show a linewidth of approximately 300 kHz,[27] with similar values found for both lighter and heavier clusters over at least two octaves of frequency.[28,29] This corresponds to 2×10^{-7} HWHM, and is very close to the measured HWHM of 10^{-7} of FT-MW machines with coaxially aligned pinhole expansions.[13] As the absolute width is much higher than at MW frequencies, we add a comment on coherence times. A linewidth of 300 kHz corresponds to a coherence time of 1 μs, which would not be sufficient for the proposed experiment. This value should be considered a lower bound, however, as the measured width includes effects that do not affect coherence (such as Doppler and time-of-flight broadening) and because the part of the beam closest to the nozzle where collisional effects are greatest was probed.[27] By moving slightly away from the nozzle and only exciting molecules once they are in the free expansion part of the jet, collisional effects would be minimized and coherence times much increased, but with the advantage that the density now drops much slower than for a pinhole expansion. As Doppler broadening is suppressed in slit jets, the ultimate limit on the linewidth would come from the time of flight through the THz beam. For a cavity with a 1 m focal length, the diameter of the beam at 1 THz is 2 cm. For a perpendicular orientation and a He jet, which has a beam velocity of about 10^5 cm/s, this would give a traversal time of 20 μs. Only recording after the ringdown occurs, this would still give $\sim 17-18$ μs of recording time and a line widths of $\sim 50-60$ kHz. The cost for this will be pumping speed, as the Mach disk will need to be at $> 3-4$ cm. Backed by a combination roots blower/mechanical pumps, a $2''/0.001''$ continuous slit jet-expansion in our lab is capable of a ~ 2 cm Mach disk, which if run in pulsed mode should provide a sufficient increase in size.

More generally, what the above analysis indicates is that as higher source power becomes available, cavities at THz frequencies should be capable of operating at similar levels, and eventually even outperform cavities at MW frequencies in terms of output coupling power. For pulsed molecular beam studies, where the duty cycle is dictated primarily by the valve/slit operating characteristics, it may be possible in FT-THz machines to match the frequency characteristics of the radiation source to the cavity. In this case, short pulses of

light would not be required and the power in the cavity could be built up to steady state levels before introducing the molecules and switching off the radiation field.

Finally, we compare the noise levels of heterodyne receivers at THz frequencies versus MW frequencies to derive relative figures of merit for FT-MW and FT-THz instruments. The noise power level of a heterodyne receiver is given by

$$P_{\text{noise}} = k_B T_{\text{rcvr}} \Delta v \tag{26}$$

where k_B is the Boltzmann constant, T_{rcvr} is the noise temperature of the receiver and Δv is the detection bandwidth. The receiver temperature T_{rcvr} thus captures the characteristics of the detector that determine the noise level. For a quantum noise-limited heterodyne receiver, T_{rcvr} is related to the frequency of the radiation through

$$k_B T_{\text{rcvr}} = \frac{hv}{\eta}, \tag{27}$$

where h is Planck's constant and η is the quantum efficiency of the detector, that is, the fraction of the photons actually recorded by the detector as signal. What this relationships shows is that if the quantum efficiency remains the same, T_{rcvr} and thus noise power of a heterodyne detector scales with frequency, which represents a significant loss in going from the MW to the THz regime. However, in both cases the detector is also exposed to thermal background noise from the cavity from which the detector cannot be shielded without also eliminating molecular signal. Therefore the overall *system* temperature T_{sys}, must include this thermal noise, and cooling the cavity mirrors can therefore lead to significant improvements in sensitivity. Indeed, the latest generation of FT-MW instruments therefore makes accommodations for LN_2 cooling of the cavity mirrors.[14] For our purposes the addition of the thermal noise to the overall system temperature has the advantage that it lowers the noise *ratios* between between the THz and MW domains. A further part of the difference can be overcome overcome through engineering efforts in increasing the quantum efficiency of THz detectors.

Indeed, much progress has been made in the design of heterodyne receivers at THz frequencies and the comparison is much improved from the situation mentioned above. A typical FTMW machines operates with a low noise front-end amplifiers, and commercially available broadband units have noise figures of 2.0 dB at room temperature (298 K) and 1.3 dB at liquid nitrogen temperatures (77 K).[14] When adding the thermal noise, this corresponds to receiver temperatures of $T_{\text{sys}} = 472$ K at room temperature and $T_{\text{sys}} = 181$ K when cooled to liquid nitrogen temperatures, respectively. At THz frequencies, T_{rcvr} values of 350–450 K at 1–1.4 THz have been achieved with superconductor-insulator-superconductor (SIS) mixers,[30] and approximately 35–40 K has been achieved at 230 GHz for ALMA Band 6 receivers (ALMA Memo #553, see http://www.alma.nrao.edu) in the 230 GHz atmospheric window. Even so, these numbers are significantly higher than quantum-limited performance, and so further improvement can be expected. For example, the fundamental quantum limit for heterodyne detection imposes a sensitivity floor of $T_{\text{rcvr}} = hv/k \sim 150$ K at 3 THz. Even when adding thermal noise to the above numbers, we see that when comparing room temperature (300 K) cavities, the detection systems in FT-MW outperform those likely to be available for FT-THz systems, but only by a factor of a few up to frequencies beyond 1–2 THz.

C. Future directions

The cavity designs presented here promise exceptional performance in FT-THz applications with pulsed molecular beams and sensitive heterodyne receivers, *provided* sufficiently intense THz radiation sources are available. While diode multiplier chain-driven local oscillators (LOs) likely possess sufficient output to enable FT-THz implementations up to several hundred GHz (if not 1 THz), scaling these devices into the 3–10 THz range, where many weakly bound clusters and biomolecules possess strong and dynamically interesting large amplitude vibration-rotation-tunneling modes, is a daunting challenge. Quantum cascade lasers (QCLs) now operate well into the THz regime, and in the best of cases provide continuous wave output powers in excess of 1 mW.[31]

The pace of THz QCL development is striking. Active frequency stabilization of these devices was achieved some time ago,[32] and recently the first THz transceiver package was reported.[33] By incorporating the QCL emitter and diode heterodyne mixer into a single, integrated package, the overall system design of FT-THz (and other) systems becomes vastly simplified. The current state-of-the-art in THz transceiver design is significantly worse than separated LO/receiver systems, but rapid improvement on this front can be expected.

Further, because cavity dispersion is so much less important at THz frequencies, rapid frequency modulation of the QCL at the cavity free spectral range could generate frequency combs that illuminate several to several tens of cavity modes simultaneously. By slightly adjusting the LO frequency from a given cavity mode frequency after illumination of the cavity, the $>$ GHz intermediate frequency response bandwidth of heterodyne detectors and modern digital oscilloscopes should provide equivalent bandwidth coverage at THz frequencies (even on single molecular beam pulses). If combined piezoelectric/stepper motor stacks are used to control the cavity length, scanning speeds of hundreds of GHz/h can be envisioned for optimized FT-THz instruments.

ACKNOWLEDGMENTS

The authors would like to thank the anonymous reviewer for several corrections and useful feedback that was used to much improve the manuscript. This work was funded, in part, by the NASA APRA program, Grant No. NNX-10AC77G, and the NSFCRIF:ID program, Grant No. CHE-0722330. R.B. is further supported by an Omidyar Fellowship.

[1]G. A. Blake, in *Encyclopedia of Chemical Physics and Physical Chemistry*, edited by J. Moore and E. Spencer (Institute of Physics, Bristol, 2000), pp. 31–44.
[2]P. H. Siegel, IEEE Trans. Microwave Theory Tech. **50**, 910 (2002).
[3]M. Tonouchi, Nat. Photonics **1**, 97 (2007).
[4]Virginia Diodes, Inc., http://vadiodes.com.
[5]S. Matsuura, G. A. Blake, R. A. Wyss, J. C. Pearson, C. Kadow, A. W. Jackson, and A. C. Gossard, Appl. Phys. Lett. **74**, 2872 (1999).
[6]J. E. Bjarnason, T. L. J. Chan, A. W. M. Lee, E. R. Brown, D. C. Driscoll, M. Hanson, A. C. Gossard, and R. E. Muller, Appl. Phys. Lett. **85**, 3983 (2004).
[7]D. C. Lis *et al*., Astron. Astrophys. **521**, L9 (2010).
[8]H. Gupta *et al*., Astron. Astrophys. **521**, L47 (2010).
[9]J. C. Lopez, M. I. Pena, M. E. Sanz, and J. L. Alonso, J. Chem. Phys. **126**, 191103 (2007).
[10]J. L. Alonso, C. Perez, M. E. Sanz, J. C. Lopez, and S. Blanco, Phys. Chem. Chem. Phys. **11**, 617 (2009).
[11]G. Berden, R. Peeters, and G. Meijer, Int. Rev. Phys. Chem. **19**, 565 (2000).
[12]T. J. Balle and W. H. Flygare, Rev. Sci. Instrum. **52**, 33 (1981).
[13]J.-U. Grabow, W. Stahl, and H. Dreizler, Rev. Sci. Instrum. **67**, 4072 (1996).
[14]J.-U. Grabow, E. S. Palmer, M. C. McCarthy, and P. Thaddeus, Rev. Sci. Instrum. **76**, 093106 (2005).
[15]L. A. Surin, B. S. Dumesh, F. Lewen, D. A. Roth, V. P. Kostromin, F. S. Rusin, G. Win newisser, and I. Pak, Rev. Sci. Instrum. **72**, 2535 (2001).
[16]A. I. Meshkov and F. C. DeLucia, Rev. Sci. Instrum. **76**, 083103 (2005).
[17]M. Y. Tretyakov, V. V. Parshin, M. A. Koshelev, M. P. Shkaev, and A. F. Krupnov, J. Mol. Spectrosc. **238**, 91 (2006).
[18]P. F. Goldsmith, *Quasioptical Systems: Gaussian Beam Quasioptical Propagation and Applications* (Wiley, New York, 1998).
[19]A. G. Fox and T. Li, Bell Syst. Tech. J. **40**, 453 (1961).
[20]J. R. Wait, Appl. Sci. Res. B, 393 (1955).
[21]J. D. Jackson, *Classical Electrodynamics* (IEEE, New York, 1999).
[22]*CRC Handbook of Chemistry and Physics*, edited by D. R. Lide, 76th ed. (CRC, Boca Raton, FL, 1995).
[23]E. J. Campbell, L. W. Buxton, T. J. Balle, and W. H. Flygare, J. Chem. Phys. **74**, 813 (1980).
[24]G. A. Blake, K. B. Laughlin, R. C. Cohen, K. L. Busarow, D. H. Guo, C. A. Schmutten maer, D. W. Steyert, and R. J. Saykally, Rev. Sci. Instrum. **62**, 1693 (1991).
[25]R. Bumgarner, S. Suzuki, P. A. Stockman, P. G. Green, and G. A. Blake, Chem. Phys. Lett. **176**, 123 (1991).
[26]K. Liu, R. J. Fellers, M. R. Viant, R. P. McLaughlin, M. G. Brown, and R. J. Saykally, Rev. Sci. Instrum. **67**, 410 (1996).
[27]K. L. Busarow, G. A. Blake, K. B. Laughlin, R. C. Cohen, Y. T. Lee, and R. J. Saykally, J. Chem. Phys. **89**, 1268 (1988).
[28]G. A. Blake and R. E. Bumgarner, J. Chem. Phys. **91**, 7300 (1989).
[29]S. Suzuki and G. A. Blake, Chem. Phys. Lett. **229**, 499 (1994).
[30]A. Karpov, D. Miller, F. Rice, J. A. Stern, B. Bumble, H. G. LeDuc, and J. Zmuidzinas, IEEE Trans. Appl. Supercond. **17**, 343 (2007).
[31]B. S. Williams, S. Kumar, Q. Hu, and J. L. Reno, Electron. Lett. **42**, 89 (2006).
[32]A. Betz, R. T. Boreiko, B. S. Williams, S. Kumar, and Q. Hu, Opt. Lett. **30**, 1837 (2005).
[33]M. C. Wanke, E. Young, C. Nordquist, M. Cich, A. Grine, C. Fuller, J. Reno, and M. Lee, Nat. Photon. **4**, 565 (2010).